Inorganic Chemistry

Article

pubs.acs.org/IC

Theoretical Insight into the Structural Stability of $KZnB_3O_6$ Polymorphs with Different BO_x Polyhedral Networks

Lei Yang,[†] Weiliu Fan,*[,‡] Yanlu Li,[†] Honggang Sun,[†] Lei Wei,[†] Xiufeng Cheng,[†] and Xian Zhao*[,†]

[†]State Key Laboratory of Crystal Materials and [‡] School of Chemistry and Chemical Engineering, Shandong University, Jinan 250100, China

Supporting Information

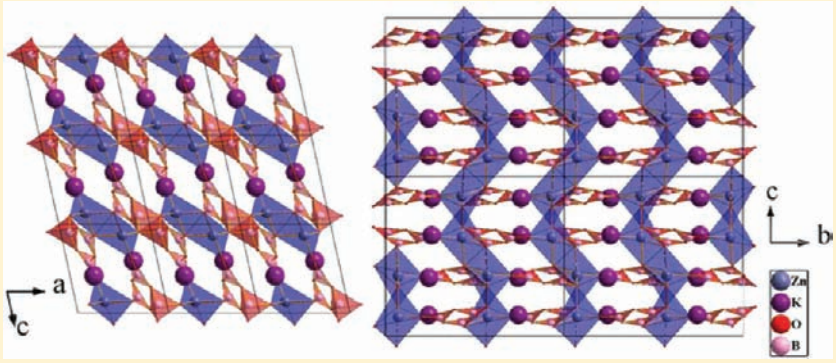

ABSTRACT: In general, the presence of shared edges of polyhedra for high-valence low-coordinated small cations is rarely seen except under extreme conditions such as high pressure. However, the ambient-pressure synthesis of $KZnB_3O_6$ built of edge-sharing BO_4 tetrahedra is contrary to this. By investigating the molecular dynamics, lattice dynamics, and electronic properties via density functional theory, we studied the origin of the phase stability of the edge-sharing (es) and "corner-sharing (cs)" $KZnB_3O_6$. Lattice dynamics results show that there are no phonon anomalies that could lead to the instability of es-$KZnB_3O_6$, which is consistent with molecular dynamics analysis. For "cs-$KZnB_3O_6$", a soft mode at the G point in the phonon dispersion is identified that reflects the dynamic instability with respect to small distortions. Eigenvector analysis of the soft mode of "cs-$KZnB_3O_6$" indicates that the instability comes from the linkage of ZnO_5 polyhedra rather than BO_x polyhedra. Electronic property calculation indicates that the edge-sharing BO_4 polyhedra connected by the longest B−O σ bonds provide a solid framework for es-$KZnB_3O_6$. In the case of "cs-$KZnB_3O_6$", the overlong Zn−O bond possesses the smallest covalent nature and the least orbital overlap among the bonds in a ZnO_5 polyhedron, and these two features of the electronic structure reduce the stability of "cs-$KZnB_3O_6$" compared to es-$KZnB_3O_6$. The electronic property calculation further confirms the results obtained from lattice dynamics analysis.

1. INTRODUCTION

Borate crystals have been intensively studied for their broad significant application in nonlinear optics materials,[1,2] fluorescent materials,[3] and laser crystals.[4] Their excellent properties are determined by their distinctive crystal structures, which have received considerable attention for more than 70 years. Up to now, the crystal structures of 1000 borates have been determined and some accepted fundamental principles have been summarized.[5−10]

As concluded from abundant borates previously discovered, there are two bonding types between B and O atoms, the BO_3 triangle and the BO_4 tetrahedron.[7] According to Paulin's third and fourth rules[11] and the orbital interpretation rules,[12] sharing of edges and particularly faces by two anion polyhedra may increase the repulsion between adjacent anions and cations, resulting in low stability of the ionic structure. In 1967, Ross and Edwards proposed that BO_3 and BO_4 groups can only exist isolated or linked by common corners.[6] This hypothesis was accepted until Huppertz and van der Eltz synthesized $Dy_4B_6O_{15}$ with an edge-sharing BO_4 structure under high pressure (HP, 8 GPa).[13] Since then, several other HP borates built of edge-sharing BO_4 tetrahedra have been synthesized, such as α-$(RE)_2B_4O_9$ (RE = Eu, Gd, Tb, Dy),[14] $RE_4B_6O_{15}$ (RE = Dy, Ho),[15] and HP-$Ni_2B_2O_4$.[16] It is generally accepted that edge-sharing BO_4 tetrahedra only form in extreme conditions such as HP.[10] However, $KZnB_3O_6$ with edge-sharing BO_4 tetrahedra was synthesized under ambient pressure[17] and could be well preserved from room temperature up to its melting point (near 1073 K) and down to 30 K. The synthesis of edge-sharing (es-) $KZnB_3O_6$ under ambient pressure unquestionably challenges the fundamental principles of borate crystal chemistry.

Jin's calculation confirmed that edge-sharing $KZnB_3O_6$ is indeed energetically more favorable than another hypothetical

Received: March 1, 2012
Published: June 5, 2012

   dx.doi.org/10.1021/ic300469s | *Inorg. Chem.* 2012, 51, 6762−6770

structure of $KZnB_3O_6$, "corner-sharing (cs-) $KZnB_3O_6$".[17,18] The latter compound does not exist; it is derived from element replacement of the existing compound $KCdB_3O_6$, which is the corner-sharing analogue to es-$KZnB_3O_6$. The result illustrates that the existence of ambient-atmosphere es-$KZnB_3O_6$ is not an accident but a certain event of energy minimization. A total energy comparison is often adopted to examine polymorphism and metastability; however, such a phenomenological approach cannot clarify the essential origin of phase stability. In order to gain further insight into the fundamental understanding of borate structures and the origin of their stability, it is necessary to investigate the network of polyhedra. One way to study the above information is to analyze the lattice dynamics properties because soft phonon modes provide details of polyhedral vibrational properties associated with structural instability. On the other hand, electronic property calculation can shed further light into the electronic origin of the soft phonon modes. In most cases, the peculiarities of the electronic structures determine the phase stability of materials because the bonds in the polyhedra that can be analyzed by electronic property calculation contribute most to the strength of the structures. Hence, lattice dynamics and electronic property analysis are of great importance in the investigation of the phase stability and the design of new structures of borates.

In this work, we also take "cs-$KZnB_3O_6$" as a hypothetical model of $KZnB_3O_6$ to make a comparison with es-$KZnB_3O_6$. First-principles calculations are presented on the molecular dynamics (MD), lattice dynamics, and electronic properties of es-$KZnB_3O_6$ and "cs-$KZnB_3O_6$" associated with their structural stabilities. The remainder of the paper is organized as follows. The first section is devoted to computational details. In the second section, the results of the above calculations are presented and discussed. The last section contains the main conclusions.

2. COMPUTATIONAL METHODS

Calculations were performed using the plane-wave pseudopotential density functional theory (DFT) method embedded in the *CASTEP* package.[19] We used a norm-conserving pseudopotential[20] and the local density approximation (LDA) with the Ceperley–Alder form[21] parametrization to describe the exchange and correlation potentials. The plane-wave cutoff energy was set at 900 eV. On the basis of the Monkhorst–Pack scheme,[23] the sizes of the *k*-point meshes for Brillouin zone sampling of primitive cells were 4 × 4 × 4 for es-$KZnB_3O_6$ and 4 × 4 × 2 for "cs-$KZnB_3O_6$". The tolerance for the self-consistent field, maximal force, maximum displacement, and maximum stress were set at 1.0×10^{-5} eV/atom, 0.03 eV/Å, 0.001 Å, and 0.05 GPa, respectively. The Mulliken populations were investigated for two equilibrium structures,[24,25] which were widely applied to perform charge transfers and bond population analysis. All property computations were obtained based on the optimized structures. The phonon frequencies and density of states (DOS) were calculated by a linear-response method.[26] Because dipole–dipole interactions affect interatomic force constants in an ionic crystal, longitudinal-optical (LO) phonons have larger frequencies than transverse-optical (TO) phonons. In order to obtain accurate frequencies and point out the influence generated by ionic displacements, we took into consideration the influence of LO–TO splitting on the modes near the G point.

In order to confirm the compounds' stability at finite temperatures, MD simulations were performed from their optimized geometry in the NPT ensemble with a time step of 1 fs over an overall period of 20 ps for es-$KZnB_3O_6$ and 1 ps for "cs-$KZnB_3O_6$". A Nosé thermostat was applied to control the temperature, which was set at 100 K intervals from 100 to 1000 K. The cutoff energy and size of the *k*-point mesh settings were consistent with those in structure optimization.

3. RESULTS AND DISCUSSION

Geometric Structures and MD. By minimization of the total energy, the equilibrium lattice parameters of es-$KZnB_3O_6$, "cs-$KZnB_3O_6$", and $KCdB_3O_6$ are derived and are listed in Table 1. Computational results demonstrate that the lattice

Table 1. Lattice Parameters of es-$KZnB_3O_6$, "cs-$KZnB_3O_6$", and $KCdB_3O_6$ with the Energy Difference per Formula Unit[a]

	a (Å)	*b* (Å)	*c* (Å)
es-$KZnB_3O_6$	6.648 (6.753)	6.920 (6.911)	7.002 (7.045)
"cs-$KZnB_3O_6$"	7.258	7.258	11.752
$KCdB_3O_6$	7.473	7.473	12.125

[a]The experimental results (ref 17) are denoted in parentheses.

constants of es-$KZnB_3O_6$ are in good agreement with experiments[17,22] (error less than 1.6%), indicating that the calculated parameters used are acceptable. The structure optimization of "cs-$KZnB_3O_6$" converges well, and its lattice constants are a little larger than those of $KCdB_3O_6$ after replacement of the Cd atoms with Zn atoms. There are no differences in the coordination environment of the atoms or the linkage type of polyhedra between "cs-$KZnB_3O_6$" and $KCdB_3O_6$.

The es-$KZnB_3O_6$ structure has triclinic symmetry with the $P\bar{1}$ space group, while the "cs-$KZnB_3O_6$" structure has monoclinic symmetry with the $C2/c$ (C_{2h}) space group (see Figure 1a,b).

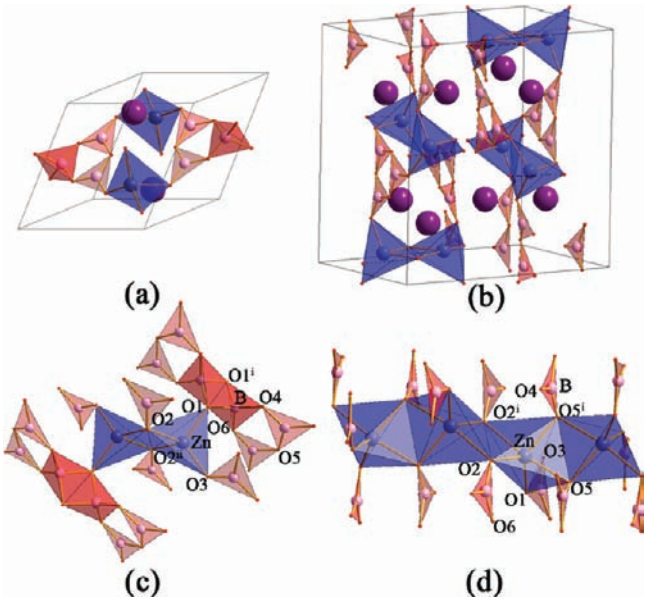

Figure 1. Optimized crystal structures of (a) es-$KZnB_3O_6$, (b) "cs-$KZnB_3O_6$", and fragments of (c) es-$KZnB_3O_6$ and (d) "cs-$KZnB_3O_6$". The gray, purple, rose, and red spheres represent Zn, K, B, and O atoms, respectively. Symmetry codes: (i) $x + 2, -y + 1, -z$; (ii) $-x + 1, -y + 2, -z$; (iii) $-x - 1, -y + 1, -z$; (iv) $-y + 2, -x + 1, -z + {}^1/_2$.

The fragment pictures (Figure 1c,d) of the two structures are given for a better understanding of the linkage type between polyhedra. The symmetry codes (represented by Roman numerals) are derived from the corresponding symmetry operations against the atoms that are not labeled with Roman numerals. The es-$KZnB_3O_6$ structure can be described as a three-dimensional framework constituted of BO_3 triangles, BO_4 tetrahedra, and ZnO_4 tetrahedra, and every two BO_4 tetrahedra

dx.doi.org/10.1021/ic300469s | Inorg. Chem. 2012, 51, 6762–6770

bind together by sharing the O1···O1^{i} edge (see Figure 1c). Different from es-$KZnB_3O_6$, "cs-$KZnB_3O_6$" is built of BO_3 triangles and ZnO_5 polyhedra. One ZnO_5 polyhedron is connected to five BO_3 triangles by different O vertexes (O1, O2, O2^{iii}, O5, and O5^{iv}) and two other ZnO_5 polyhedra by the O2···O2^{iii} and O5···O5^{iv} edges, as illustrated in Figure 1d. The ZnO_5 polyhedra connect with each other in a zigzag chain along the *c* axis, which determines the structure stability along the *c* axis.

MD simulations of both structures were implemented to confirm their phase stability at finite temperature. It is found that the es-$KZnB_3O_6$ structure is well preserved up to 1000 K and down to 100 K, with no bond breaking or large distortion over a period of 20 ps (shown in Figure 2a). In the case of "cs-$KZnB_3O_6$", the longest Zn−O bonds (2.259 Å) in "cs-$KZnB_3O_6$" stretch to a very large extent (about 3.8 Å) within 1 ps, resulting in the extremely weak linkage between ZnO_5 polyhedra and the large distortion of the "cs-$KZnB_3O_6$" structure (shown in Figure 2b). As the temperature improves, the "cs-$KZnB_3O_6$" structure deforms more quickly. Because that 1 ps is long enough to reflect its potential instability, we did not present a 20-ps-long MD calculation for "cs-$KZnB_3O_6$" like we did for es-$KZnB_3O_6$ considering the vast computational cost.

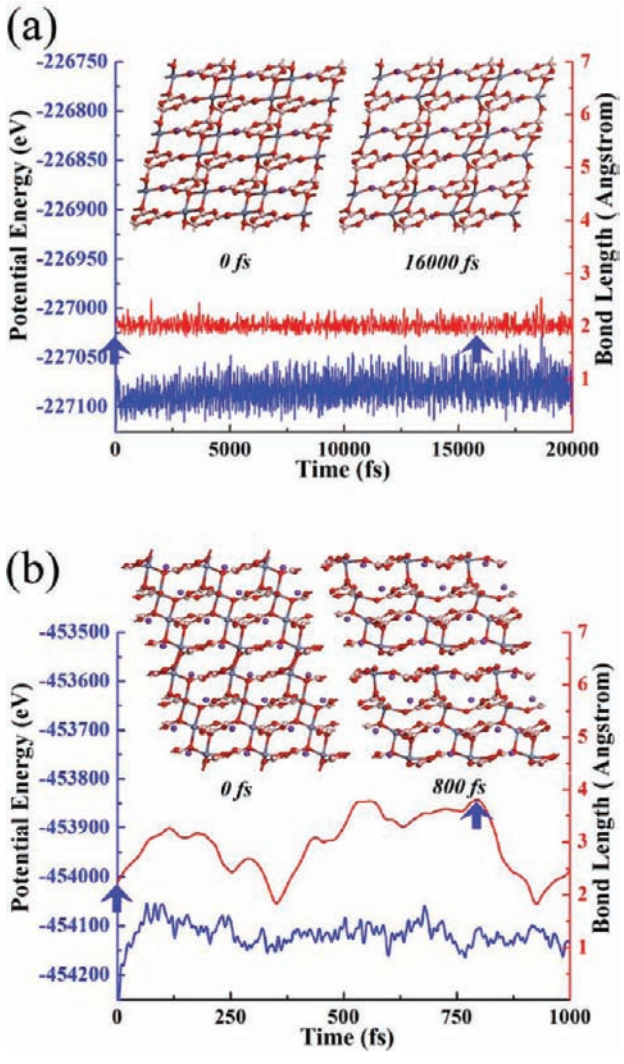

Figure 2. Potential energy (blue line) and the longest Zn−O bond length (red line) as a function of the time of MD simulation of es-$KZnB_3O_6$ (a) and "cs-$KZnB_3O_6$" (b) with their structures at the beginning (left) and after a certain time with MD runs (right) at 1000 K.

Lattice Dynamics. Lattice dynamics properties were performed within the density functional perturbation theory.[26,27] The calculated phonon dispersion relations along high-symmetry directions and phonon DOS for es-$KZnB_3O_6$ and "cs-$KZnB_3O_6$" are illustrated in Figure 3a,b, respectively.

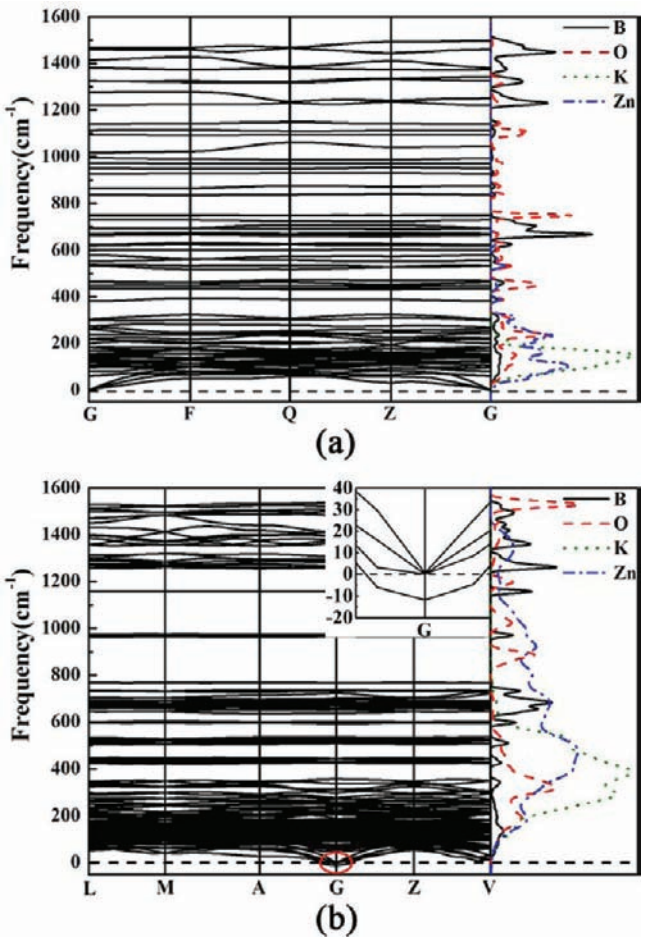

Figure 3. Phonon dispersion and partial phonon DOS for (a) es-$KZnB_3O_6$ and (b) "cs-$KZnB_3O_6$". In part b, imaginary frequencies are plotted on the negative axis, and the inset shows dispersion curves in the red ellipse.

For es-$KZnB_3O_6$, there are no soft modes at any wave vectors, indicating that es-$KZnB_3O_6$ is stable at 0 K. In contrast, a notable soft mode (11.7 cm^{-1}) is observed at the G point in the phonon dispersion of "cs-$KZnB_3O_6$", which adequately demonstrates its dynamic instability. In order to verify whether the imaginary frequency at the G point is the inherent characteristic of "cs-$KZnB_3O_6$", we have performed a frequency calculation by *DMol*,[3] with the data listed in S1 in the Supporting Information. The imaginary frequency at the G point calculated by *DMol*[3] is 14.8 cm^{-1}, indicating that the imaginary frequency is not caused by other factors. The spectra of the two structures can be divided into three separate bands: the low-frequency region (below 360 cm^{-1}, containing acoustic and low optical bands), the medium-frequency region (360−780 cm^{-1}), and the high-frequency region (above 780 cm^{-1}).

dx.doi.org/10.1021/ic300469s | *Inorg. Chem.* 2012, 51, 6762−6770

Table 2. Calculated and Experimental Phonon Frequencies (cm^{-1}) with the Assignment for es-$KZnB_3O_6$

IR (A_u)		Raman (A_g)		
present	experiment (ref 14)	present	experiment (ref 14)	assignment
1442.4	1442	1460.0	1455	BO_3 stretching modes
1414.7/1369.5	1384	1381.6		
1309.7	1304	1324.5		
1276.4/1227.7	1240	1219.8		BO_4 stretching modes
1109.8		1141.0	1130	
		1094.8		
1015.3	1000			BO_4 bending modes
991.6				
968.4		951.1		
		927.3		
863.7	870	836.8	850	
746.4	723	750.0	767	BO_4 and BO_3 bending modes
		728.9		
689.5		695.0		BO_3 bending modes
669.4		667.9		
663.5				
621.2		621.9		
		601.4		
		580.3	585	
554.1				ZnO_4 stretching modes and BO_3 bending modes
531.4		533.6	533	
467.5		462.5	462	ZnO_4 bending modes and BO_3 bending modes
448.9				
435.7		436.9	430	
		381.9	375	ZnO_4 bending modes, translational and rotational modes of BO_3, and edge-sharing BO_4
301.6		300.2		
267.1		263.2	253	
261.2/242.9				
231.2				
219.5		216.1		
		200.2		K atom translational modes, ZnO_4 bending modes, translational and rotational modes of BO_3, and edge-sharing BO_4
176.7		181.7		
		166.1		
151.7		154.2		
143.4		145.6		
137.4		127.6		
		119.9		
106.2		106.4		
96.1		80.9		
		60.3		

Combined with the phonon DOS analysis for both structures, it is found that the low-frequency regions are mainly contributed by Zn and K atoms because of their heavier atomic masses, while the high-frequency vibrations mainly come from B atoms, which are lighter. Meanwhile, the vibrations of O atoms are distributed in the whole region of the spectra. It can be seen that the high-frequency region of the phonon dispersion of es-$KZnB_3O_6$ appears more dispersive than that of "cs-$KZnB_3O_6$". As presented in Figure 3, for "cs-$KZnB_3O_6$", the phonon DOS of O and B atoms in the high-frequency region have sharp peaks at 970, 1160, and 1260 cm^{-1}, while in the spectra of es-$KZnB_3O_6$, discriminative peaks disperse and become smaller. The distinction between the two phonon dispersions is caused by the existence of BO_4 modes in es-$KZnB_3O_6$, whose frequencies fill in the blanks between the frequencies of BO_3 stretching and bending modes.

The es-$KZnB_3O_6$ primitive unit cell contains 22 atoms, leading to 66 degrees of freedom at the Brillouin zone center. Our calculated frequencies are in good agreement with the experimental data,[17] except for being a little higher in some modes in the high-frequency region (see Table 2). The LDA method overall underestimates the volume of the primitive unit cell, resulting in the fact that some computed frequencies are higher than those in experiments. The irreducible representation of the $P\bar{1}$ space group at the G point yields a sum of $3A_u$ for acoustic modes and $30A_u + 33A_g$ for 63 optical modes, where A_u is IR-active and A_g is Raman-active. The IR- and Raman-active modes are mutually exclusive because of the centrosymmetry of the structure. The mixed ionic−covalent nature of the chemical bonding of es-$KZnB_3O_6$ results in the split of three IR-active modes A_u into three longitudinal A_u (LO) and three transverse A_u (TO), whose frequencies are 261.2/242.9, 1276.4/1227.7, and 1414.7/1369.5 cm^{-1}, respec-

dx.doi.org/10.1021/ic300469s | Inorg. Chem. 2012, 51, 6762−6770

Table 3. Calculated Phonon Frequencies (cm^{-1}) with the Assignment for "cs-$KZnB_3O_6$"

IR		Raman		
A_u	B_u	A_g	B_g	assignment
1516.7	1486.8	1538.0	1509.2	BO_3 stretching modes
1469.2/1397.9	1393.6	1413.6	1408.8	
1374.2	1388.7/1362.6	1374.4	1370.3	
1285	1276	1295.8	1284.5	
1263.5	1259	1259.4	1265.1	
1159.4	1159.6	1158.7	1159.0	
973.7	970.2	975.3	972.0	BO_3 stretching and bending modes
966.5	964.9	968.1	968.3	
767.1	766.3	767.1	766.2	BO_3 bending modes
731.9		735.2	723.1	
	696.7			
677.4	688.8	684.1	678.6	
670.3		675.9	674.6	
659.0	658.4		657.5	
	651.2	638.4		
603.4	596.0	601.5	594.5	
527.2	523.4	537.4	535.1	ZnO_5 stretching modes and BO_3 bending modes
520.3	507	525.1	511.5	
443.9	444.2	445	445.8	ZnO_5 and BO_3 bending modes
430.7	427.3	430.2	428.0	
	358.3		338.4	ZnO_5 bending modes and BO_3 translational and rotational modes
315.3		315.0		
300.3				
		278.1	273.1	
	273.2/257.8	251.0	258.8	
249.8	244.3	237.3		
225.9		215.6	227.0	
211.8	206.6	190.4		K atom translational modes, ZnO_5 bending modes, and BO_3 translational and rotational modes
180.1	179.5	183.4	184.1	
172.8	167.3	164.9	173.9	
154.8	155.7	153.0	152.5	
			151.3	
145.7			146.5	
	139.8	136.4	143.6	
131.6	128.9			
125.1	121.4	125	120.7	
111.5		110.4		
111.0		106.2	108.4	
	90.9		96.9	
		78.3	73.5	
66.0	62.1	60.9	53.7	
	11.7i			

tively. In the case of "cs-$KZnB_3O_6$", there are 44 atoms in a primitive unit cell, generating 132 phonon modes at the G point (Table 3). The irreducible representation of the $C2/c$ space group is $A_u + 2B_u$ for three acoustic modes and $32A_u + 33A_g + 31B_u + 33B_g$ for 129 optical modes. Selection rules state that the A_u and B_u modes are IR-active, whereas the A_g and B_g modes are Raman-active. There are three IR-active modes, A_u (1469.2/1397.9 cm^{-1}) and $2B_u$ (273.2/257.8 and 1362.6/1362.6 cm^{-1}), of "cs-$KZnB_3O_6$" splitting into LO and TO components.

In order to investigate the further origin of the structural stability, we have analyzed the assignment for the modes for both structures. According to Huppertz,[15] there are two Raman-active ranges of the edge-sharing BO_4 tetrahedral modes in the HP borate cases at about 1253−1271 and 1431−1444 cm^{-1}. For es-$KZnB_3O_6$, we observe that the modes in 1094−1460 cm^{-1} are attributed to stretching of the edge-sharing BO_4 tetrahedra and the BO_3 triangles. Figure 4 shows the eigenvectors for the vibrational patterns of A_g at 1141 and 1460 cm^{-1}, which can be assigned to the internal stretching modes of BO_4 and BO_3. All of the vibrational frequencies of the edge-sharing BO_4 tetrahedra are in the high-frequency region rather than in the imaginary region, indicating that the vibrational modes of edge-sharing BO_4 tetrahedra are dynamically stable.

Unlike es-$KZnB_3O_6$, the high-frequency region frequencies of "cs-$KZnB_3O_6$" at the G point are more concentrated, as discussed in phonon dispersion and DOS because of the large difference between the frequencies of BO_3 stretching and bending modes. In the medium- and low-frequency regions, the frequencies of the ZnO_5 polyhedral modes in "cs-$KZnB_3O_6$" are

dx.doi.org/10.1021/ic300469s | Inorg. Chem. 2012, 51, 6762−6770

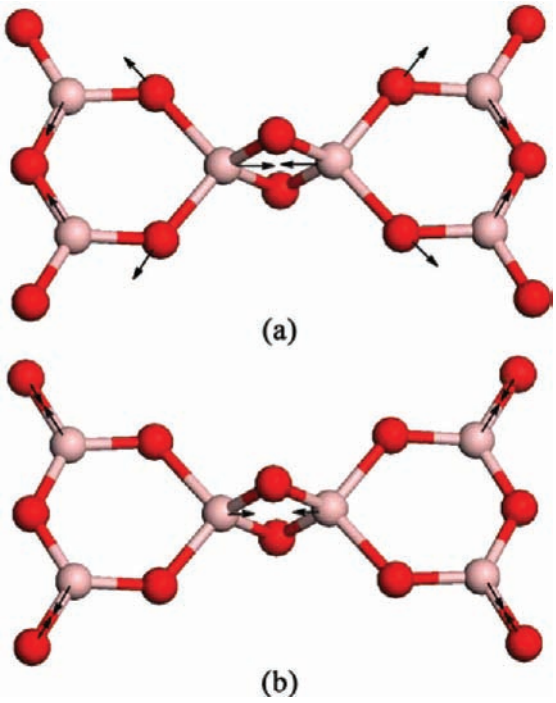

Figure 4. Atom eigenvectors for the vibrational modes of A_u in BO_x groups of es-$KZnB_3O_6$ (a) at 1141 cm^{-1} and (b) at 1460 cm^{-1} (rose and red spheres represent B and O atoms, respectively).

lower than those of the ZnO_4 polyhedral modes in es-$KZnB_3O_6$ because the former have longer bond lengths.

The soft mode present in the structure of "cs-$KZnB_3O_6$" does not vanish under either positive or negative pressure. From Figure 5, it can be clearly seen that adjacent ZnO_5

Figure 5. Atom eigenvectors for the vibrational modes of B_u at 11.7i cm^{-1} in ZnO_y groups of "cs-$KZnB_3O_6$" (gray and red spheres represent Zn and O atoms, respectively).

polyhedra move in opposite directions accompanied by the shear displacement of two adjacent planes when relaxing along the eigenvectors of the soft mode. This results in the breakage of the longest Zn−O bonds and finally the separation of the two ZnO_5 polyhedra. This analytical method of the eigenvectors of soft modes is always applied in a displacive-type ferroelectric phase transition.[28] Because of the instability of the framework provided by ZnO_5 polyhedra, "cs-$KZnB_3O_6$" cannot exist in normal conditions.

Electronic Structures. To gain a further understanding of the phase stability, we performed analysis of the corresponding Mulliken charge and bond populations of the two structures, and the results are listed in Table 4. It is known that the absolute magnitudes of the atomic charges derived by population analysis have little physical meaning, but some valuable information can be found from the relative values of the Mulliken populations. From Table 4, it can be seen that in both structures the charges transferred from Zn, K, and B atoms to O atoms are about 1.2 e, 1.0 e, and −0.8 e, respectively.

For BO_x groups, the B−O bonds in the BO_4 polyhedra of es-$KZnB_3O_6$ are longer and less covalent than those in the BO_3 triangles of es-$KZnB_3O_6$ and "cs-$KZnB_3O_6$" because of the increased repulsion between O atoms when the fourth B−O bond is added. The B−O bonds (B−O1, 1.499 Å; B−$O1^{i}$, 1.486 Å) between two B atoms are even longer than the other two (B−O4, 1.437 Å; B−O6, 1.442 Å) in the BO_4 polyhedra of es-$KZnB_3O_6$ because of the repulsion of B···B between the two BO_4 polyhedra. Among the O atoms connected with Zn atoms of es-$KZnB_3O_6$, the ones forming the common edge of the BO_4 polyhedra get less charge (−0.75 e).

For ZnO_y groups, the charge value of Zn atoms of es-$KZnB_3O_6$ (1.19 e) is smaller than that of "cs-$KZnB_3O_6$" (1.22 e). In addition, the Zn−O bonds of "cs-$KZnB_3O_6$" are longer than those of es-$KZnB_3O_6$. Among the Zn−O bonds of es-$KZnB_3O_6$, Zn−$O2^{ii}$ (2.002 Å) and Zn−O2 (2.080 Å) are a little longer and have a less covalent nature than the other two (Zn−O1, 1.980 Å; Zn−O3, 1.943 Å). Every ZnO_4 connects with another one through the common edge. In the case of es-$KZnB_3O_6$, the longest Zn−O5 bond (2.259 Å, shown in Figure 1d) is not much longer than the second longest one (Zn−$O2^{iii}$, 2.231 Å), whereas the other three in the same plane are about 2 Å. The Zn−O5 and Zn−$O2^{iii}$ bonds possess a less covalent nature than the other three. Owing to the Zn−O5 and Zn−$O2^{iii}$ bonds, the ZnO_5 polyhedra connect together with each other and form a chain. In other words, every ZnO_5 polyhedron shares its edges with two others in "cs-$KZnB_3O_6$". At the same time, the common O...O edge of two ZnO_5 polyhedra is shortened by the Coulomb repulsion between Zn atoms to an extent of 14%. Such a large distortion can not be ignored when considering the stability of "cs-$KZnB_3O_6$". Apart from two edge-sharing ZnO_5 polyhedra, five BO_3 triangles are connected to the same Zn atom. These groups repel each other due to the steric hindrance effect, resulting in the stretching of Zn−O5 bonds.

The calculated band structures and DOS spectra of es-$KZnB_3O_6$ and "cs-$KZnB_3O_6$" are illustrated in Figures 6 and 7. It can be seen that both es-$KZnB_3O_6$ and "cs-$KZnB_3O_6$" are wide-gap semiconductors with indirect band gaps of 4.292 and 4.328 eV. The direct band gaps at the highly symmetric G point of es-$KZnB_3O_6$ and "cs-$KZnB_3O_6$" are 4.462 and 4.355 eV, respectively. The results may be underestimated owing to the well-known limitation of the DFT method. As shown in Figure 7, the tops of the valence band are dominated by O 2p states in both structures and the bottoms of the conduction band are mainly composed of Zn 4s states. The increase of the lowest energy of Zn 4s states results in a larger band gap of "cs-$KZnB_3O_6$", as shown in Figure 7b.

For a further understanding about the bonding character related to the phase stability, we plotted the charge-density contour maps and stereopictures corresponding to the selected state regions marked with ellipses (A−D and a−c) in the DOS of Figure 7, as illustrated in Figures 8 and 9. In the region of −8.2 to −7.6 eV of the DOS of es-$KZnB_3O_6$, a B atom binds to four O atoms with four stable σ bonds, whose states form from the B sp^3-hybridized states and O 2p states, as shown in the stereopicture in Figure 8a. Hence, in the case of es-$KZnB_3O_6$, although the new B−O σ bonds may introduce latent instability

dx.doi.org/10.1021/ic300469s | Inorg. Chem. 2012, 51, 6762−6770

Table 4. Atomic and Bond Populations for es-$KZnB_3O_6$ and "cs-$KZnB_3O_6$"[a]

es-$KZnB_3O_6$					"cs-$KZnB_3O_6$"				
species	charge	bonds	population	length	species	charge	bonds	population	length
		B−O bonds in BO_3					B−O bonds in BO_3		
B1	0.76	B−O	0.74−0.97	1.328−1.402	B1	0.73	B−O	0.77−1.03	1.316−1.396
B2	0.81	B−O bonds in BO_4			B2	0.78			
B3	0.81	B−O1	0.56	1.499	B3	0.81			
O1	−0.75	B−O1[i]	0.57	1.486	O1	−0.81			
O2	−0.81	B−O4	0.69	1.437	O2	−0.79			
O3	−0.82	B−O6	0.67	1.442	O3	−0.73	Zn−O bonds in ZnO_5		
O4	−0.73	Zn−O bonds in ZnO_4			O4	−0.72	Zn−O1	0.43	1.983
O5	−0.74	Zn−O1	0.30	1.980	O5	−0.79	Zn−O2	0.32	2.020
O6	−0.72	Zn−O2	0.22	2.080	O6	−0.71	Zn−O2[iii]	0.16	2.231
K	1.01	Zn−O2[ii]	0.30	2.002	K	1.00	Zn−O5	0.12	2.259
Zn	1.19	Zn−O3	0.44	1.943	Zn	1.22	Zn−O5[iv]	0.30	2.025

[a]Symmetry codes: (i) $x + 2, -y + 1, -z$; (ii) $-x + 1, -y + 2, -z$; (iii) $-x - 1, -y + 1, -z$; (iv) $-y + 2, -x + 1, -z + {}^1/_2$.

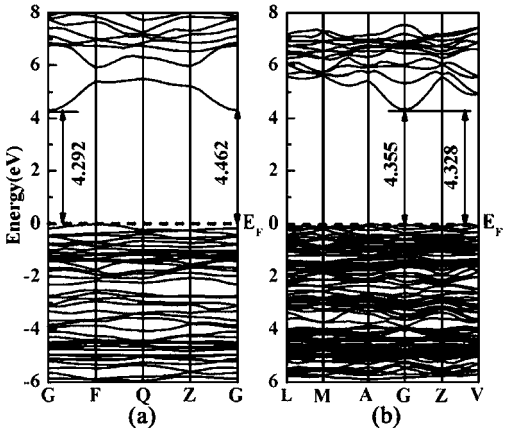

Figure 6. Band structures of (a) es-$KZnB_3O_6$ and (b) "cs-$KZnB_3O_6$".

in the edge-sharing region as analyzed in Jin's deformation electron-density slice,[17] they still provide a solid frame by which es-$KZnB_3O_6$ can stably exist. In the region of −7.6 to −6.8 eV, we can infer that the states of the 3-fold-coordinated B atom are sp^2-hybridized and the σ-bonding states form from O 2p and B sp^2-hybridized states from Figure 9A. The Zn−O σ-bonding states shown in Figure 9B form from Zn 3d and O 2p states in the region of −5.9 to −2.1 eV. Besides the σ framework in BO_3, the large π^*-antibonding states that are formed from the parallel p obitals of the B and O atoms are observed, as shown in Figure 8b (the region of 5−8 eV).

In the case of "cs-$KZnB_3O_6$", the compositions of states are the same as those of es-$KZnB_3O_6$ in the regions of −7.6 to −6.8, −5.9 to −2.1, and 5−8 eV, and their charge-density contour maps are illustrated in Figures 9C, 99D, and 8c, respectively. The difference of the B−O coordination types between two structures is exhibited in the region of −8.2 to

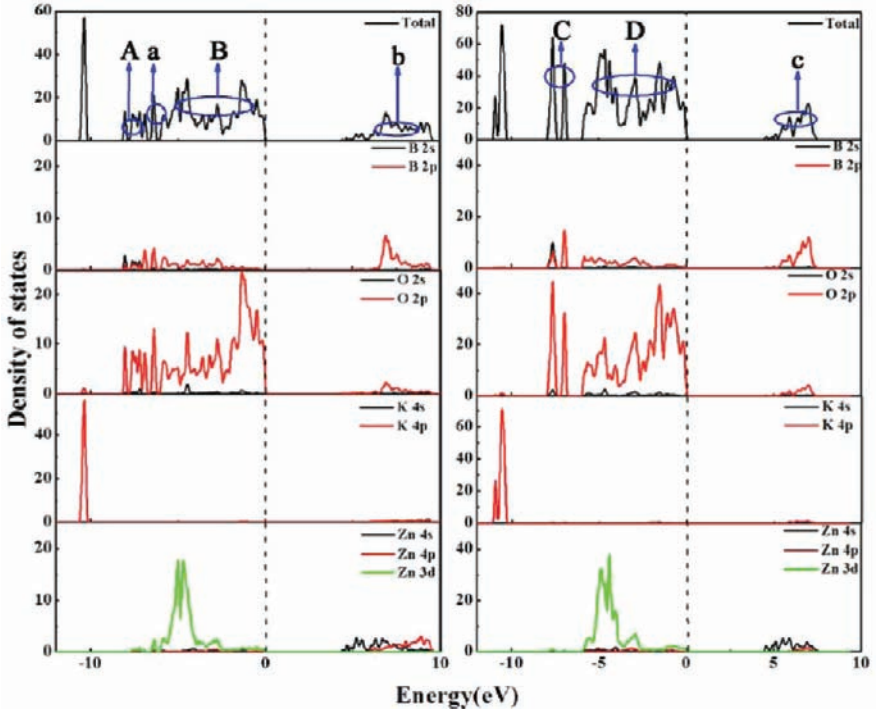

Figure 7. Total and partial DOS of es-$KZnB_3O_6$ (left) and "cs-$KZnB_3O_6$" (right).

dx.doi.org/10.1021/ic300469s | Inorg. Chem. 2012, 51, 6762−6770

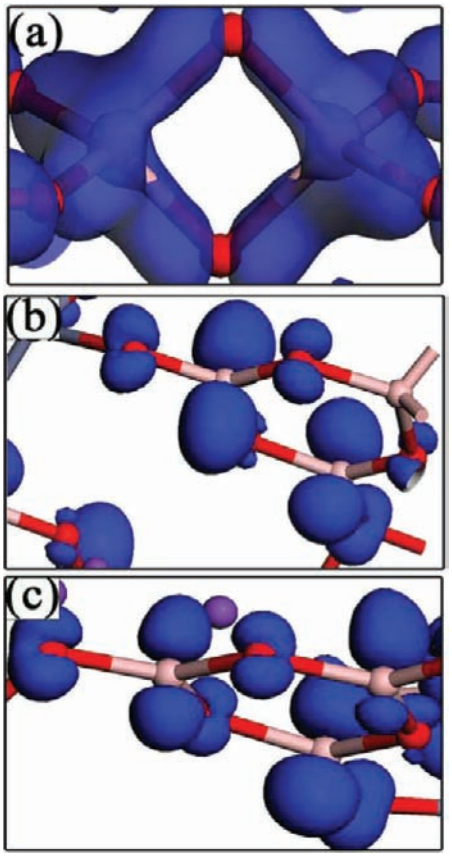

Figure 8. Stereopictures for various electronic states of B−O bonds in es-$KZnB_3O_6$ and "cs-$KZnB_3O_6$" corresponding to the selected energy range (a−c) marked with an ellipse in the DOS.

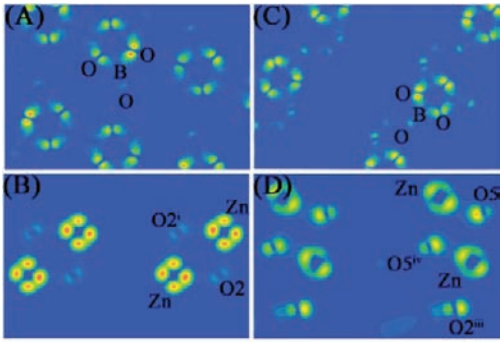

Figure 9. Charge-density contour maps for various electronic states of the B−O and Zn−O bonds in es-$KZnB_3O_6$ and "cs-$KZnB_3O_6$" corresponding to the selected energy range (A−D) marked with an ellipse in the DOS.

−7.6 eV, where the states of some B atoms are sp^3-hybridized in es-$KZnB_3O_6$ while those in "cs-$KZnB_3O_6$" are still sp^2-hybridized. Moreover, in the case of "cs-$KZnB_3O_6$" (Figure 9D), the least orbital overlap between Zn 3d and O 2p states is observed in the Zn−O5 bond. This overlong Zn−O5 bond also possesses the smallest covalent nature in a ZnO_5 polyhedron, and these two features of the electronic structure reduce the stability of "cs-$KZnB_3O_6$" compared to es-$KZnB_3O_6$. Hence, the electronic property analysis not only confirms the conclusion drawn from the lattice dynamics but also locks the phase instability of "cs-$KZnB_3O_6$" in the longest Zn−O bonds.

4. CONCLUSION

Via DFT, we have performed a systematic investigation on the MD, lattice dynamics, and electronic properties of edge-sharing $KZnB_3O_6$ and "corner-sharing $KZnB_3O_6$" associated with structural stabilities. MD simulations show that, from 100 to 1000 K, es-$KZnB_3O_6$ is stable enough to be preserved, while "cs-$KZnB_3O_6$" deforms with bond stretching. From analysis of lattice dynamics, we infer that the vibrational modes of edge-sharing BO_4 tetrahedra are dynamically stable and all modes have real frequencies in es-$KZnB_3O_6$. In the case of "cs-$KZnB_3O_6$", a soft mode at the G point (B_u) with an imaginary frequency of 11.7 cm^{-1} is found. Eigenvector analysis of the soft mode shows that the linkage of ZnO_5 polyhedra is dynamically unstable. The electronic structures of es-$KZnB_3O_6$ and "cs-$KZnB_3O_6$" are quite different because of the different coordinations of B and Zn atoms. In a BO_4 polyhedron, one B atom binds to four O atoms with four stable σ bonds, whose states form from the B sp^3-hybridized states and O 2p states. The longest B−O σ bonds that connect the edge-sharing BO_4 polyhedra are stable enough to provide a solid framework for es-$KZnB_3O_6$. In the case of "cs-$KZnB_3O_6$", two edge-sharing ZnO_5 polyhedra and five BO_3 triangles are connected to the same Zn atom, and they repel each other because of steric hindrance and the Coulomb repulsion effect, resulting in the stretching of the Zn−O5 bond. The Zn−O5 bond possesses the smallest covalent nature and the least orbital overlap in a ZnO_5 polyhedron, indicating its instability. It is exactly these overlong Zn−O bonds that cause a decrease of the force constant, leading to the soft mode of ZnO_5 polyhedra in "cs-$KZnB_3O_6$". That is, the structure instability of "cs-$KZnB_3O_6$" comes from the linkage type of the ZnO_5 polyhedra rather than from the BO_x polyhedra, which is consistent with MD analysis. The results of this study strongly support clarification of the structural stability origination of $KZnB_3O_6$, indicating that the approaches of lattice dynamics and electronic property analysis for polyhedral networks are valid. As supplements to Pauling's rules, these approaches will help in the design of new structures of borate materials.

■ ASSOCIATED CONTENT

Ⓢ Supporting Information

Frequencies at the G point of "cs-$KZnB_3O_6$". This material is available free of charge via the Internet at http://pubs.acs.org.

■ AUTHOR INFORMATION

Corresponding Author

*E-mail: fwl@sdu.edu.cn (W.F.), zhaoxian@icm.sdu.edu.cn (X.Z.). Tel: 86-531-88366330. Fax: 86-531-88364864.

Notes

The authors declare no competing financial interest.

■ ACKNOWLEDGMENTS

This work is supported by the National Natural Science Foundation of China (Grants 91022034 and 51172127) and the Excellent Youth Foundation of Shandong Scientific Committee (Grant JQ201015). Thanks go to Dr. Edward C. Mignot, Shandong University, for linguistic advice.

■ REFERENCES

(1) He, M.; Chen, X. L.; Okudera, H.; Simon, A. *Chem. Mater.* **2005**, *17*, 2193−2196.

(2) Xu, Z. Y.; Liu, X.; Deng, D. Q.; Wu, Q.; Wu, L. A.; Wu, B. C.; Lin, S. J.; Lin, B.; Chen, C. T. *J. Opt. Soc. Am. B* **1995**, *12*, 2222−2228.
(3) Wu, L.; Chen, X. L.; Li, H.; He, M.; Xu, Y. P.; Li, X. Z. *Inorg. Chem.* **2005**, *44*, 6409−6414.
(4) Li, X. Z.; Wang, C.; Chen, X. L.; Li, H.; Jia, L. S.; Wu, L.; Du, Y. X.; Xu, Y. P. *Inorg. Chem.* **2004**, *43*, 8555−8560.
(5) Christ, C. L. *Am. Mineral.* **1960**, *45*, 334−340.
(6) Ross, V. F.; Edwards, J. O. The Structural Chemistry of the Borates. In *The Chemistry of Boron and its Compound*; Muetterties, E. L., Ed.; John Wiley: New York, 1967.
(7) Christ, C. L.; Clark, J. R. *Phys. Chem. Miner.* **1977**, *2*, 59−87.
(8) Filatov, S. K.; Bubnova, R. S. *Phys. Chem. Glasses* **2000**, *41*, 216−224.
(9) Becker, P. *Z. Kristallogr.* **2001**, *216*, 523−533.
(10) Filatov, S. K.; Bubnova, R. S. Structural Mineralogy of Borates as Perspective Materials for Technological Applications. In *Minerals as Advanced Materials I*; Krivovichev, S. V., Ed.; Springer: Berlin, 2008.
(11) Pauling, L. *J. Am. Chem. Soc.* **1929**, *51*, 1010−1026.
(12) Burdett, J. K.; McLarnan, T. J. *Am. Mineral.* **1984**, *69*, 601−621.
(13) Huppertz, H.; von der Eltz, B. *J. Am. Chem. Soc.* **2002**, *124*, 9376−9377.
(14) Emme, H.; Huppertz, H. *Chem.—Eur. J.* **2003**, *9*, 3623−3633.
(15) Huppertz, H. *Z. Naturforsch.* **2003**, *58 b*, 278−290.
(16) Knyrim, J. S.; Roessner, F.; Jakob, S.; Johrendt, D.; Kinski, I.; Glaum, R.; Huppertz, H. *Angew. Chem., Int. Ed.* **2007**, *46*, 9097−9100.
(17) Jin, S. F.; Cai, G. M.; Wang, W. Y.; He, M.; Wang, S. C.; Chen, X. L. *Angew. Chem., Int. Ed.* **2010**, *49*, 4967−4970.
(18) Jin, S. F.; Cai, G. M.; Liu, J.; Wang, W. Y.; Chen, X. L. *Acta Crystallogr., Sect. C* **2009**, *65*, i42−i44.
(19) Clark, S. J.; Segall, M. D.; Pickard, C. J.; Hasnip, P. J.; Probert, M. J.; Refson, K.; Payne, M. C. *Z. Kristallogr.* **2005**, *220*, 567−570.
(20) Hamann, D. R.; Schluter, M.; Chiang, C. *Phys. Rev. Lett.* **1979**, *43*, 1494−1497.
(21) Ceperley, D. M.; Alder, B. J. *Phys. Rev. Lett.* **1980**, *45*, 566−569.
(22) Wu, Y.; Yao, J. Y.; Zhang, J. X.; Fu, P. Z.; Wu, Y. C. *Acta Crystallogr., Sect. E* **2010**, *66*, i45.
(23) Monkhorst, H. J.; Pack, J. *Phys. Rev. B* **1976**, *13*, 5188−5192.
(24) Sanchez-Portal, D.; Artacho, E.; Soler, J. M. *Solid State Commun.* **1995**, *95*, 685−690.
(25) Segall, M. D.; Shah, R.; Pickard, C. J.; Payne, M. C. *Phys. Rev. B* **1996**, *54*, 16317−16320.
(26) Gonze, X. *Phys. Rev. B* **1997**, *55*, 10337−10354.
(27) Baroni, S.; de Gironcoli, S.; dal Corso, A.; Giannozzi, P. *Rev. Mod. Phys.* **2001**, *73*, 515−562.
(28) Moriwake, H.; Kuwabara, A.; Fisher, C. A. J.; Taniguchi, H.; Itoh, M.; Tanaka, I. *Phys. Rev. B* **2011**, *84*, 104114.